PROCEEDINGS OF SCIENCE

Enabling technologies for X-ray transients monitoring from Moon- and satellite-based observatories

Francesco Ceraudo*

INAF-IAPS,
Via del Fosso del Cavaliere, 100, 00133, Roma, Italy

E-mail: francesco.ceraudo@inaf.it

The transient emission of astrophysical sources can shed some light onto the most extreme conditions matter can be exposed to in the universe, which are not reproducible on Earth. Current established technologies, such as small-field-of-view grazing-incidence optics and Charged Coupled Devices, are inadequate in this context, as they do not ensure the required grasp, sensitivity and throughput necessary to observe bright transients, and to discover and monitor known or new sources. In this paper, I will be reviewing some new technologies and proposed mission concepts for the study of astrophysical X-ray transients from space, both on board satellites and from the surface of the Moon. All presented instruments are based on the sensor technology of Silicon Drift Detectors coupled with new-generation optical systems, with the goal of solving current technological limitations.

Frontier Research in Astrophysics - IV (FRAPWS2024)
9-14 September 2024
Mondello, Palermo, Italy

*Speaker

 ISSN 1824-8039 . Published by SISSA Medialab.

PoS(FRAPWS2024)068

1. Introduction

After a brief introduction of the scientific context (Sec. 1.1) and of the state of the art of current technologies and their limitations and possible solutions (Sec. 1.2), I will present several instrument concepts: the PixDD project (Sec. 2), the Large Area Detector (Sec. 3), the HERMES constellation (Sec. 4), the Wide Field Monitor (Sec. 5) and the LEM-X observatory (Sec. 6). In each section, plentiful references will be listed for further details.

1.1 Scientific context

With the routine detection of gravitational waves [1], and most especially the simultaneous observation of an electromagnetic counterpart [2–4], astrophysics has entered the *multi-messenger era*, in which more traditional photon-based studies are complemented by gravitational wave and neutrino observatories [5, 6]. Most of the candidate phenomena for multi-messenger studies give rise to transients, i.e. evolving emissions that can be very bright and may develop on very limited timescales (e.g. fractions of seconds as in short Gamma-Ray Bursts), whose position and time of occurrence cannot be predicted. Besides the multi-messenger context, transient sources open windows on the most extreme conditions in the universe, especially those occurring in the proximity of compact objects, that cannot be reproduced on Earth [7–9]. Together with the growing detection volume of current and future observatories, the unpredictability of transients poses a challenge to the ability to match detections across different instruments, in order to get as a complete view as possible of the phenomena. Fortunately, photon transient are rarer in the energy band from X-rays to γ-rays, a fact that boosts the probability of finding electromagnetic counterparts to astrophysical phenomena detected with other means. Efficient and responsive X-ray instruments capable of continuously monitoring large portions of the sky with good localization accuracy on a wide range of time scales, as well as of fluxes, therefore represent an important tool in the new multi-messenger era. Likewise, the ability to follow the spectral and time evolution of already discovered sources may unveil the physics behind their working mechanisms.

To this landscape, one must add the renewed international interest in the Moon, as a platform for further scientific exploration, both with ground-based structures and satellite-borne payloads [10–14].

1.2 Technological landscape

The scientific goals highlighted in Sec. 1.1 require instruments operating in the energy range between a few keV and a few MeV, with good spectral ($< 500\,\mathrm{eV}$ at $6\,\mathrm{keV}$) and time ($< 10\,\mu\mathrm{s}$) resolution, as well as photon-by-photon capabilities, in order to be able to follow the spectral and time evolution of the transient emission. Good sensitivity ($< 1\,\mathrm{Crab}$ in $1\,\mathrm{s}$) is also an important requirement, both to quickly accumulate statistical significance and for a fast identification of sources in preparation for follow-up studies. On the other hand, pile-up probability should be kept low even in the case of bright events, in order to take advantage of all available data.

In the following sections, I will provide a very brief overview to both traditional and new-generation optical systems for the study of transients in the X-ray band (Sec. 1.2.1), followed by an outline of current detector technology and its shortcomings in this context (Sec. 1.2.2). Finally, I

will introduce Silicon Drift Detectors (Sec. 1.2.3), the technology at the core of all the instruments detailed in the rest of this paper.

1.2.1 Optical systems for high-energy transients

Instruments for the study of transients fall into two very broad categories, featuring large and small fields of view (FOVs). The first family is mainly employed for the discovery and identification of unknown transients, as well as for the continuous monitoring of astrophysical sources known to undergo transient phases. The second group of instruments is instead used mainly for follow-up studies, as the probability of a burst occurring in a small field of view is very low.

In both cases, traditional multilayer grazing reflection optics [15] show severe drawbacks that prevent their effective employment. Despite being a well-established technology [16–19] that can be adapted to operate in a large energy range ($< 80\,\mathrm{keV}$) with excellent angular resolution and sensitivity, this family of optics has a cripplingly small effective-area-to-mass ratio, requiring very heavy systems with very long focal lengths in order to reach the effective area necessary to study transients. Moreover, their very small FOV ($< 1^\circ$) makes this optical system unsuitable for the discovery of unknown sources.

For the aforementioned reasons, alternative solutions have been proposed, e.g. arrays of short-focal-length low-resolution multilayer optics (concentrators), and collimators for small-FOV instruments, as well as *lobster-eye* optics and coded-masks for large-FOV telescopes. The use of a distributed architecture based on multiple independent systems has also become a viable option in recent years.

1.2.2 Limitations of current detectors

Despite being the most widespread detector in X-ray astronomy for their excellent energy and spatial resolution, Charge Coupled Devices (CCDs) suffer from important drawbacks, mainly deriving from their nature as charge-integrating devices. This indeed puts unavoidable constraints on their performances, as dead time and pile up can be a serious issue in the case of high-flux sources. Moreover, the build-up of leakage current in the pixels during integration can be contrasted with either low operating temperatures ($< -70\,^\circ\mathrm{C}$) [20–22], which may put severe strain on the whole system when power is a limited resource as in a typical satellite-borne mission, or smaller pixels, which inevitably increases the readout time and further degrades the timing performances. New technologies solve some issues while introducing other drawbacks: for example, Depleted p-channel Field Effect Transistors (DEPFETs) can reach excellent spectral resolutions and $> 10\,\mathrm{kHz}$ frame rates at the expense of an even higher power consumption [23–27].

1.2.3 Silicon Drift Detectors

Silicon Drift Detectors (SDDs) [28] represent an interesting alternative to more traditional devices, as they have the possibility to solve some of the issues highlighted above.

In an SDD, the bulk (usually n-type silicon) is fully depleted thanks to voltages applied to implanted electrodes (typically p^+-doped cathodes), which also shape the internal electric field as to funnel electrons towards the anodes. When an electron-hole cloud[1] is generated in the sensitive

[1] Number of electron-hole pairs $N_{\mathrm{eh}} = E/\omega$, where E is the deposited energy and $\omega = 3.63\,\mathrm{eV}$ in silicon.

bulk due to photoelectric effect by X-ray photons or ionization tracks of charged particles, electrons *drift* to the anodes, where they are eventually collected by the readout electronics. Holes, on the other hand, migrate to the field-shaping cathodes and recombine. The charges move with a speed of $v_{\text{drift}} = \mu\mathcal{E}$, where $\mathcal{E}$ is the electric field strength and μ is the mobility of the charge carriers ($1360\,\text{cm}^2\,\text{V}^{-1}\,\text{s}^{-1}$ for electrons and $450\,\text{cm}^2\,\text{V}^{-1}\,\text{s}^{-1}$ for holes, at 300 K), implying that for typical detector geometries the electron drift duration is well within 10 µs.

Thanks to the collecting properties of the internal electric field, various detector shapes may be adopted according to the specific need (e.g., linear, central). Moreover, the readout anodes can be made very small with respect to the active surface of the sensor, thus limiting the detector capacitance, and therefore improving the timing and spectral performances. The impact of the leakage current is limited because there are no distinct integration and readout phases, unlike in CCDs, and therefore thermal electrons do not accumulate in the detector, which further increases the spectral performances. The fact that SDDs are continuously active also implies that they only marginally suffer from effects such as pile-up and dead time. Finally, their operating energy range can be tuned to various applications: sensitivity to lower energies can be improved by selecting the proper design of the surface structures, whereas efficiency at higher energies can be changed by modifying the thickness of the bulk and possibly by coupling the SDD with other detectors, e.g. scintillators.

2. The Pixelated Silicon Drift Detector

A collaboration between the Italian National Institute for Astrophysics (INAF), the National Institute for Nuclear Physics (INFN), the Bruno Kessler Foundation (FBK), Polytechnic of Milan, University of Pavia, and the Karlsruhe Institute of Technology (KIT), the *Pixelated Silicon Drift Detector* (or PixDD) project aims to develop a high-throughput multi-pixel SDD-based detection system for spectral-timing studies to be placed at the focal plane of non-imaging soft-X-ray optics (concentrators and lobster-eye), while at the same time solving many of the limitations of current X-rays detectors. Sensitive in the 0.5 – 15 keV range, it will feature good spectroscopic performances even at room temperature or with mild cooling (FWHM $\lesssim$ 150 eV at 6 keV at 0 °C), along with a robust time resolution ($\lesssim$ 10 µs). The goal of the project is to design a compact modular system of integrated sensor and readout electronics, that can potentially be replicated to cover large focal planes such as those typical of lobster-eye optics, in a practice known as *tiling*. Table 1 lists the main requirements of the device.

2.1 Sensor

The sensor is made out of a monolithic matrix of 300 µm × 300 µm SDD pixels, whose dimensions match the typical Point Spread Functions of X-ray concentrators [29] and lobster-eye optics [30], providing the necessary oversampling. With a 450 µm-thickness and a very thin X-ray entrance window, the device is capable of detecting photons below < 10 keV with a high efficiency, while maintaining a high sensitivity even below 500 eV [31].

By taking advantage of the SDD design, the anode capacitance of each PixDD pixel can be kept to $\leq$ 35 fF, without losing charge collection efficiency. At the same time, a dedicated production process developed by FBK can lower the leakage current to levels below a few hundreds $\text{pA}\,\text{cm}^{-2}$,

Table 1: Main requirements of the PixDD integrated system.

Parameter	Value
Energy range	$0.5 - 15\,\mathrm{keV}$
Energy resolution	$< 150\,\mathrm{eV}$ at $< 6\,\mathrm{keV}$ at $< 0\,^{\circ}\mathrm{C}$
Time resolution	$< 10\,\mu\mathrm{s}$
Sensitivity	Single photon
Reading architecture	Continuous sparse readout
Operating temperature	$\geq 0\,^{\circ}\mathrm{C}$
Integration properties	Tiling

Table 2: Main characteristics of the RIGEL ASIC.

Parameter	Value
Technology	AMS $0.35\,\mu\mathrm{m}$ CMOS
Number of channels	128 (16 rows $\times$ 8 columns)
	256 (16 rows $\times$ 16 columns)
Channel pitch	$300\,\mu\mathrm{m} \times 300\,\mu\mathrm{m}$
Energy range	$0.5 - 15\,\mathrm{keV}$
Shaping times	$0.5 - 5\,\mu\mathrm{s}$
Energy threshold	$0.5 - 3\,\mathrm{keV}$
ADC Conversion time	$\approx 100\,\mu\mathrm{s}$
ADC resolution	10 bit
ENC	$\approx 10\,\mathrm{e^-_{rms}}$
Power consumption	$640\,\mu\mathrm{W/ch}$

with records of $< 50\,\mathrm{pA\,cm^{-2}}$ [32], thus allowing PixDD to have a sub-pA pixel-wise anode current. This unique combination of low anode capacitance and leakage current enables the detector to be operated at (nearly) room temperature with Fano-limited spectral resolution, as well as to reach fast readout speeds ($< 5\,\mu\mathrm{s}$) without degrading much the spectral performance.

Current prototypes of the sensor feature 4×4, 16×8, 16×16 and 32×32 pixel matrices.

2.2 ASIC

The RIGEL is the Application Specific Integrated Circuit designed to be coupled with the PixDD sensor [33]. It consists of a matrix of Readout Pixel Cells (RPCs) that match the pixels of the sensors, so that every anode can be connected to the input of an RPC. Each RPC has a complete analog readout chain: low-power continuous-reset Charge-Sensitive Amplifier, pole-zero cancellation circuit and CR-RC shaper with selectable time constants, amplitude discriminator, peak stretcher, and a pile-up rejection system. The matrix of RPCs is completed by a back-end circuitry featuring the power distribution network, the configuration memory banks, and the serial communication interface. Most importantly, for each row of the RPC matrix, the back end hosts a 10-bit Wilkinson ADC in charge of digitizing the analog output of the cells in that row. Table 2

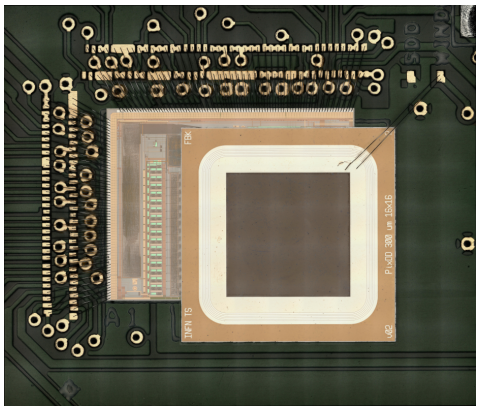

Figure 1: Picture of the integrated PixDD-RIGEL system. The 16×16 sensor is visible on top, whereas the RPC matrix of the RIGEL is below, with only the back-end portion of the ASIC emerging from the sides.

summarizes the main characteristics of the device. An important property of the RIGEL is the sparse readout, i.e. the ability of each cell to trigger and be read out independently of the others, which dramatically cuts down dead time and pile-up issues (e.g., contrary to CCDs).

The current available designs of the RIGEL ASIC allow it to be coupled with the 16×8 and 16×16 versions of the sensors. Moreover, the ASIC technology has been extensively qualified with heavy ion beams for radiation effects, both Total Ionizing Dose and Single Event Effects [34].

2.3 Bonding

To limit the parasitic capacitance that would result from wire-bonding the detector anodes to the analog inputs of the RPCs, while at the same time keeping the fill factor as high as possible, the sensor and the ASIC are bump-bonded together with a novel process that can be performed at die-level, without requiring specific lithographic processed during fabrication [35]. This technique involves first the deposition of $< 40\,\mu$m gold studs on the anodes of the sensor and the analog inputs of the RIGEL, obtained by melting the extremity of a capillary wire. After that, the two devices are heated up and pressed against each other, in order for the aligned gold studs to merge. After the bonding procedure, the integrated structure appears as shown in Fig. 1.

2.4 Measured spectral performances

The preliminary 4×4 sensor prototypes coupled with an external readout system yielded very promising results with FWHM (5.9 keV) < 150 eV already at room temperature [36, 37]. Afterwards, the 16×8 and 16×16 matrices, consisting of integrated sensor and RIGEL ASIC, were tested extensively, and produced results in line with the requirement of the instrument [38, 39]. For instance, Fig. 2 shows the results of a ^{55}Fe characterization of the 16×16 system, where a FWHM (5.9 keV) ≈ 150 eV is achieved at 0 °C for single pixels, with a median value of ≈ 160 eV across the whole matrix.

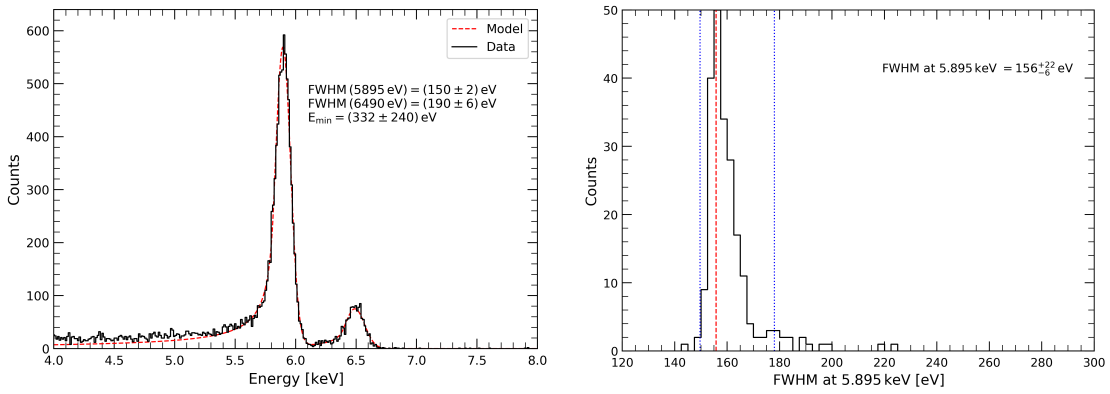

(a) **(b)**

Figure 2: Spectral resolution of the 16×16 integrated PixDD-RIGEL system, measured at the ^{55}Fe lines at 0 °C: single pixels (a), and statistical distribution across the matrix (b).

2.5 Future developments

As stated earlier, one of the main goal of the PixDD project is to create a system that can densely cover wide focal planes, such as those found in lobster-eye optics. In order to achieve this, the current design must be improved in two major ways.

1. The inactive area of the guard rings along the periphery of the sensor must be dramatically decreased. Those structures allow in fact to degrade the electric potential from the active depleted interior of the detector to the inactive undepleted volume of the surrounding die. However, to be effective, they must cover a wide surface, hence reducing the fill factor of the sensitive area in the case of tiling.

2. The back-end portion of the ASIC must be removed from around the RPC matrix, since this limits how closely two structures can be placed together.

Both approaches are currently under investigation. To decrease the extension of the guard rings, and thus creating *slim-edge* or *edge-less* sensors, an innovative and promising possibility is the use of doped trenches that can carry out the same function as guard rings by taking up a smaller surface area, essentially making the rings three-dimensional (*Deep Reactive Ion Etching*, or DRIE) [40, 41]. Earlier prototypes are already available and will be tested in the next future. On the other hand, the modification of the ASIC geometry requires to split the circuit into two separate chips and then bump-bond them in order to create a three-dimensional ASIC, the necessary electrical connections between the RPCs and the back-end being also provided by *Through-Silicon Vias* [42].

3. The Large Area Detector

The *Large Area Detector* (LAD) is a narrow-field-of-view instrument concept on board proposed international missions such as LOFT [43, 44], eXTP [45, 46] and STROBE-X [47, 48], to carry out spectral-timing studies of transient X-ray sources, and unveil the properties of matter under extreme conditions of gravity and magnetism [7–9].

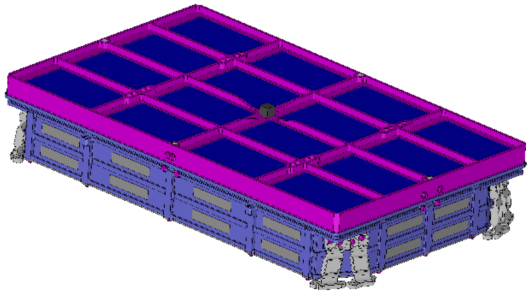

Figure 3: Design of the LAD module proposed for eXTP, featuring a set of 4×4 SDD-collimator pairs (blue rectangles on the top) [46].

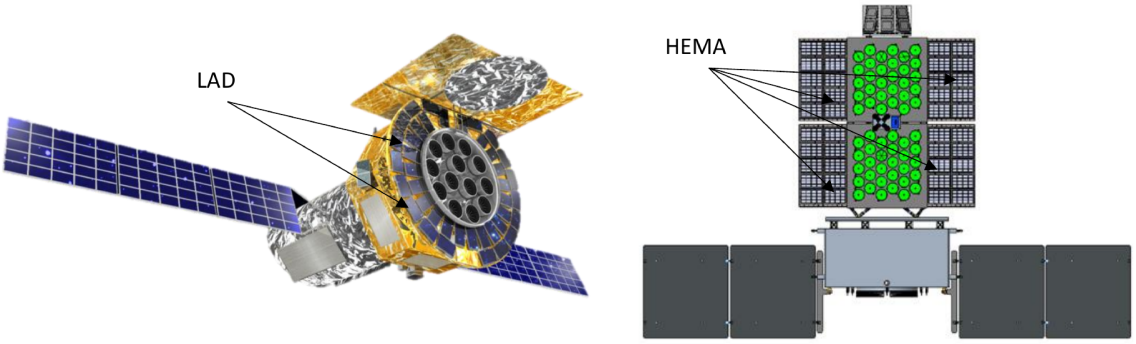

Figure 4: Artistic views of the LAD proposed on board eXTP (*left*, adapted from [46]) and STROBE-X (*right*, adapted from [49]). Each instrument features 40 modules (Fig. 3).

In order to maximize effective area while minimizing pile-up, the LAD features a large collecting surface with many readout channels, so that the count rate per channel may stay limited. The fundamental building block of the LAD is a single large-area SDD matched to a lightweight collimator of the same size, to limit the angle of acceptance of incoming photons. Sets of detector-collimator pairs are arranged into identical and almost self-sufficent *modules* (Fig. 3), allowing the LAD to be shaped according to the specific needs and room availability of the mission [50], as visible in Fig. 4.

From the description given above, the LAD emerges as a collimated rather than focused instrument. This frees its design from the constraints of long-focal lengths and bulky optics, and instead gives the freedom to increase the effective area to enormous values by simply replicating its fundamental unit. The downside of this approach is the generally higher background with respect to a focused instrument, making the LAD optimal for the observation of bright astrophysical sources. Table 3 lists the main parameters of the LAD in two proposed configurations.

3.1 Micro-Pore Optics

To define its FOV, the LAD employs Micro-Pore Optics (MPO) in the form of Capillary Plate (CP) collimators, based on the technology of Micro-Channel Plates (MCPs) [51]. Lightweight 5 mm-thick lead-rich glass plates featuring cylindrical channels with a 83 µm-diameter arranged

Table 3: Main parameters of the LAD proposed for both eXTP and STROBE-X.

Parameter	Value
Number of modules	40
Effective area	$> 1.3\,m^2$ at 2 keV
	$> 3\,m^2$ at 8 keV
	$> 1.5\,m^2$ at 30 keV
Energy range	2 – 30 keV (nominal)
	2 – 80 keV (extended)
Field of view	$< 65'$
Energy resolution	< 260 eV at 6 keV (all events)
Time resolution	10 µs
Absolute time accuracy	2 µs
Dead time	< 1 % at 1 Crab
Maximum sustained flux	> 1 Crab

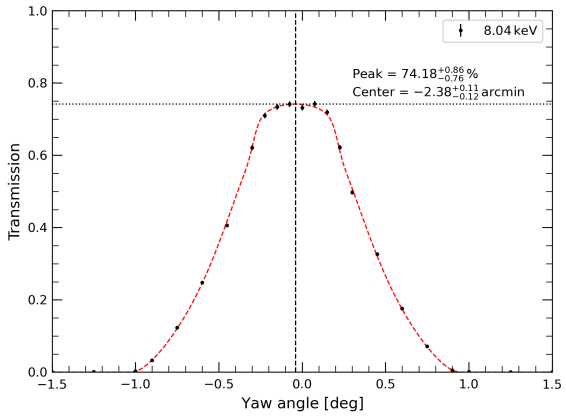

Figure 5: Angular response of a prototype of the LAD collimator. Transmission measurements take at 8.04 keV are compared to the analytical model of the response itself. The maximum transmission as well as the angle where it occurs are highlighted.

in a hexagonal fashion, absorb off-axis photons ensuring a 1°-FOV (FWHM). The weight of the collimators is limited partly thanks to the material and partly to the very high Open Area Ratio (OAR), i.e. the fraction of surface made out of empty channels, which can be > 70 %.

The development of this technology is still underway (Fig. 5). Indeed, the LAD has stringent requirements regarding the alignment between the pores, the OAR and the polishing of the inner CP channel walls, as all those parameters greatly influence the optical response of the device, and by extension that of the instrument as a whole [52–54].

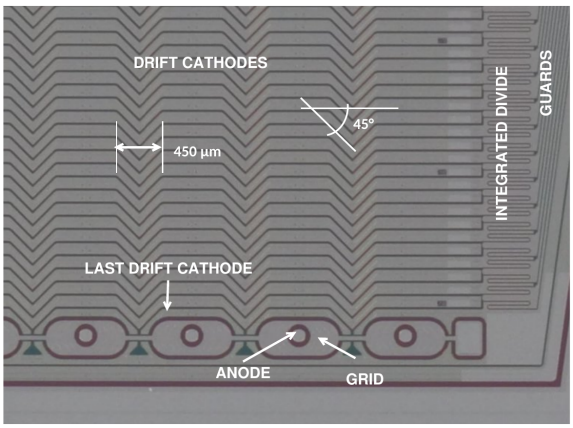

Figure 6: Design of the LAD SDD. The structures preventing the charges from spreading and focusing the electrons onto the anodes are indicated (adapted from [56]).

3.2 Large-area linear SDD

The sensitive core of the LAD is made out of a large-area linear Silicon Drift Detector, whose design is described in detail in [55] and [56], and which will be quickly outlined in the following.

Under the action of a $\approx 360\,\mathrm{V\,cm^{-1}}$ electric field, electrons generated in the sensitive bulk are pushed towards the anode lines placed along the sides of the detector, where they are collected by as many readout channels. However, due to diffusion, the charge cloud expands during the drift, assuming a Gaussian shape whose standard deviation σ is given by

$$\sigma = \sqrt{2Dt + \sigma_0^2} = \sqrt{2\frac{k_\mathrm{B}T}{q}\mu\frac{Y}{\mu\mathcal{E}} + \sigma_0^2} = \sqrt{2Y\frac{k_\mathrm{B}T}{q\mathcal{E}} + \sigma_0^2}, \tag{1}$$

where D is the diffusion coefficient, k_B is Bolzmann's constant, T is the temperature, μ is the electron mobility, q is the elementary charge, $\mathcal{E}$ is the electric field, Y is the distance from the readout region, and σ_0 is the width of the distribution before the diffusion, which is negligible for the LAD. Therefore, according to the position of the interaction, the electrons may be collected by multiple readout channels, with the consequent degradation of the spectral performances due to the multiple additions of electronic noise. To limit this phenomenon, and also to contain the capacitance that would otherwise arise from simply using fewer but bigger anodes, specifically designed field-shaping electrodes are added to prevent the charge clouds from spreading sideways, along with a focusing electric field in the charge collection region, allowing a small anode to gather all the charge. With this design (Fig. 6), the LAD sensor can feature two lines of 112 anodes each, spaced by 970 µm, and having only a capacitance of ≈ 90 fF.

Prototypes of the LAD detector show that the design described above boosts the fraction of single events (photons read out by only one electronic channel) to $> 94\,\%$, whereas double events are reduced to $< 6\,\%$, and no events have higher multiplicity. At the same time, spectral resolutions as low as 214 eV at 5.9 keV at 0 °C have been measured, with even lower values expected at lower temperatures [56].

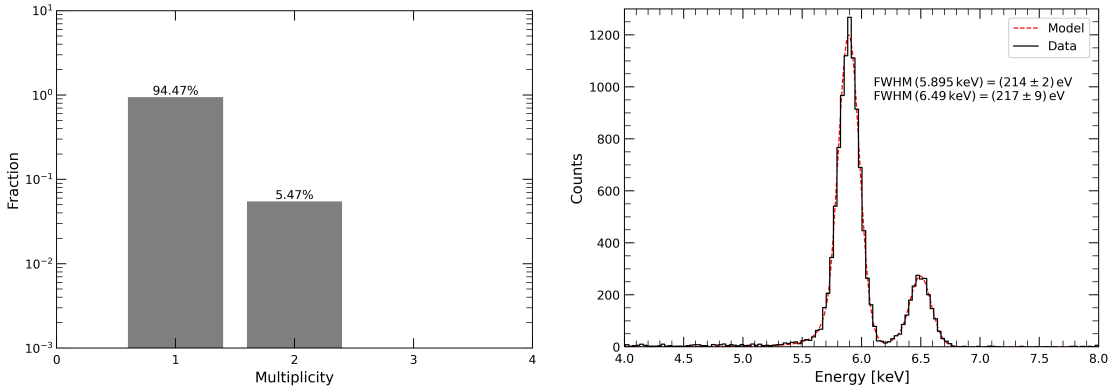

(a) **(b)**

Figure 7: Spectral performances of the prototypes of the LAD detector. Figure a: The distribution of multi-anode events shows that the majority of photons are collected by a single anode. Figure b: A spectral resolution as low as 214 eV at 5.9 keV has been measured at 0 °C (single events).

c

It is worth noting that the LAD sensor technology has been fully qualified for the space environment, i.e. displacement damage [57], Total Ionizing Dose [58] and micrometeoroids [59].

4. The High Energy Rapid Modular Ensemble of Satellites

The *High Energy Rapid Modular Ensemble of Satellites* (HERMES) is an all-sky monitor for the localization and study of high-energy transient sources in the keV to MeV band [60]. It is based on a distributed architecture, in the form of a constellation of nano-satellites (3U CubeSats) on a low Earth orbit. In its initial form as a pathfinder mission, HERMES will comprise a suite of six identical satellites, to be launched in 2025 [61]. The constellation is enriched by a further HERMES-like payload onboard the Australian *Space Industry Responsive Intelligent Thermal nano-satellite* (SpIRIT), launched in 2023 [62].

4.1 The constellation

The fast identification of transients requires large fields of view, and accurate localization for follow-up studies, two features that may be hard to combine under the mass and power constraints that are typical of space missions. A possible solution consists of forgoing altogether the idea of a single instrument to adopt instead a distributed architecture, made out of a constellation of smaller identical satellites.

With this approach, localization is performed through *triangulation* [63]. The components of the constellation are distributed in such a way that at least three of them monitor a given patch of the sky at the same time. In the event of a transient, by virtue of the relative distance between them, each satellite will detect a slightly delayed version of the same light curve: by correlating the signals, the source location can be pinpointed in the sky with an accuracy σ_{PA} which depends on the number of satellites participating in the triangulation N, their baseline D and the associated uncertainty (σ_{pos}), the error in the determination of the arrival times of the incoming photons (σ_{time})

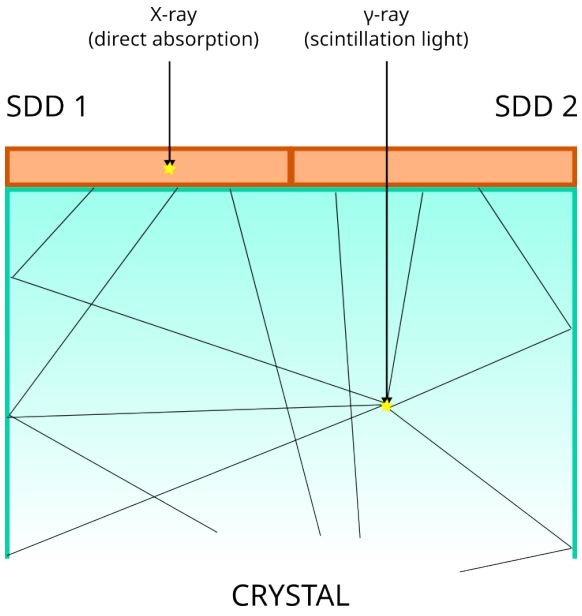

Figure 8: Working principle of the siswich detector: X-rays are directly absorbed by the outward-facing SDDs, whereas γ-rays go through the silicon detectors, interact with the crystal and illuminate the SDD from the back.

and the one deriving from the correlation process (σ_{delay}):

$$\sigma_{\text{PA}} \approx \frac{\sqrt{\sigma_{\text{delay}}^2 + \sigma_{\text{pos}}^2/c^2 + \sigma_{\text{time}}^2 + \sigma_{\text{sys}}^2}}{D\sqrt{N-1-2}}, \tag{2}$$

where σ_{sys} is a systematic error.

A distributed configuration has the obvious advantages of redundancy and modularity, as each unit can be developed and deployed independently of one another, so that even the failure of one or more of them does not necessarily jeopardize the whole system. Moreover, the constellation can be expanded over time and even upgraded by launching new modules. The advantages of this approach become even more evident if the members of the constellation are CubeSats, as in the case of HERMES. If built (mostly) of *components off-the-shelf* (COTS), i.e. commercially available items that do not require specific qualification procedures, CubeSats may dramatically cut down costs and development time to a fraction of the typical ones even for a "traditional" satellite mission, even of small size. A relatively high failure rate is somewhat expected for CubeSats, but this is abundantly compensated for by all the aforementioned advantages.

4.2 The siswich detector

Each CubeSat of the HERMES constellation, as well as SpIRIT, features a 10 cm×10 cm×10 cm (1U) scientific payload (Tab. 4) built around the *siswich* detector concept [64–67]. In this innovative architecture (Fig. 8), an SDD has one side exposed to astrophysical photons, while its other side is coupled with a scintillator (in this case a GAGG:Ce crystal) sensitive to γ-rays. When X-rays from space reach the SDD, they deposit their energy through photoelectric effect and are therefore

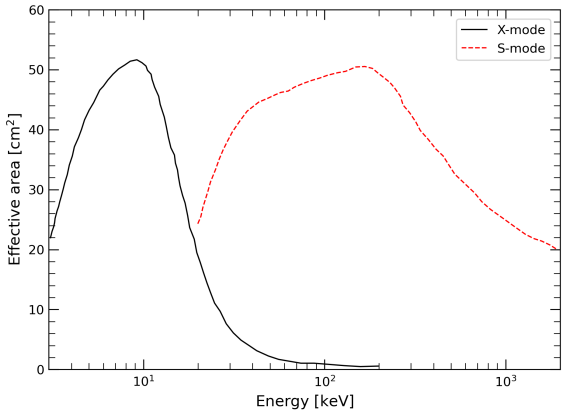

Figure 9: Effective area of the HERMES payload as a function of energy.

Table 4: Main parameters of each HERMES payload.

Parameter	Value
Payload peak effective area	52 cm^2
Field of view	3.2 sr (FWHM)
Low-energy threshold	$\leq$ 3 keV
Energy resolution	$\leq$ 800 eV at 6 keV
	$\leq$ 5 keV at 60 keV
Time resolution	320 ns (68 % c.l.)
Time accuracy	181 ns (68 % c.l.)
Mass	1.55 kg
Volume	10 cm $\times$ 10 cm $\times$ 10 cm

detected by the sensor. If the photon energy is high enough that the SDD becomes transparent, however, the photon may interact with the crystal underneath, and therefore generate visible light, which is in turn detected by the SDD itself, optically coupled with the scintillator. X-rays and γ-rays are then distinguished by pairing two SDDs with a single crystal: being point-like, photoelectric interactions only trigger a single SDD (X-mode), whereas the scintillation light illuminates both SDDs at the same time, creating a double event (S-mode). This technology greatly enhances the energy band of the HERMES detector, allowing it to space from $\approx$ 2 keV to $\approx$ 2 MeV (Fig. 9).

5. The Wide Field Monitor

The *Wide Field Monitor* (WFM) is a coded-mask instrument concept tasked with the identification and localization of X-ray transients, as well as the continuous monitoring of persistent sources. Based on independent 2 sr-FOV cameras (Tab. 5) that can be combined into different arrangements, the WFM as a whole can attain an unprecedented instantaneous FOV. Configurations based on the WFM camera have been proposed for the LOFT [68], eXTP [69], STROBE-X [70] and LEM-X

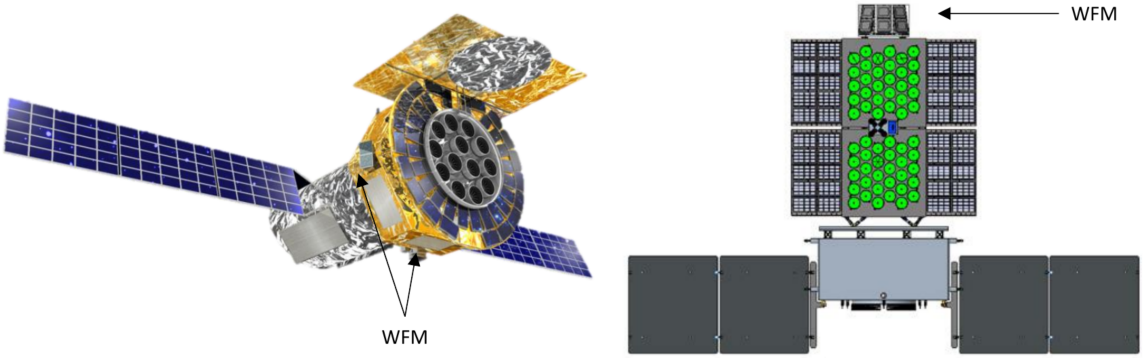

Figure 10: Artistic views of the WFM proposed on board eXTP (*left*, adapted from [69]) and STROBE-X (*right*, adapted from [49]).

Table 5: Main parameters of the WFM camera.

Parameter	Value
Energy range	2 – 50 keV
Imaging technology	Coded mask
Field of view (zero response)	$90° \times 90°$
Point Source Location accuracy	$\sim 1'$
Spatial resolution (FWHM, average, all energies)	< 25 µm (fine)
	< 6 mm (coarse)
Angular resolution (FWHM, average, all energies)	$< 5'$ (fine)
	$< 5°$ (coarse)
Energy resolution (6 keV, average, all multiplicities)	< 500 eV
Time resolution	10 µs
Sensitivity	< 1 Crab in 1 s
	< 5 mCrab in 50 ks
Volume	~ 35 cm $\times$ 35 cm $\times$ 35 cm
Mass	~ 18 kg

(Sec. 6) space missions.

5.1 1.5-D imaging

At the core of the WFM camera is a large-area SDD sharing many similarities with the one of the LAD, and as such described in detail in [55]. Further details regarding the design of the sensors as well as some simulations and experimental results are reported in [71, 72]

As it happens in the LAD, in the WFM as well the charge cloud expands during the drift under the action of diffusion, according to eq. 1. However, in this case, this is a desirable phenomenon, because, by sampling the charge profile, it is possible to estimate the position and shape of the cloud, and to reconstruct the impact position of the photon. Indeed, since the drift occurs orthogonally towards the line of the anodes, the center of the distribution along that line (X coordinate)

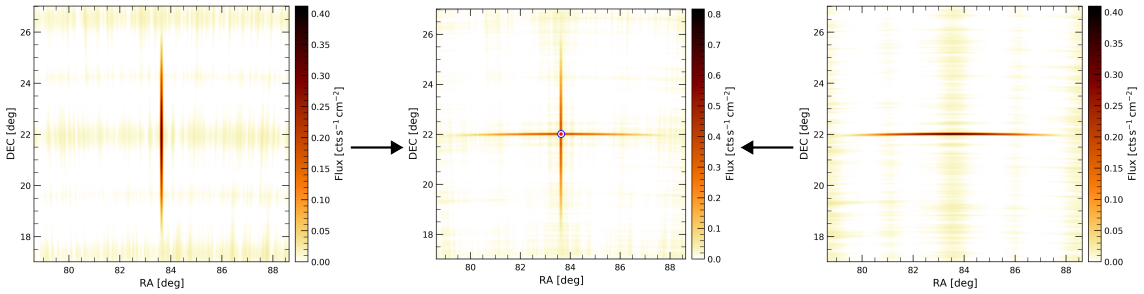

Figure 11: Source localization from the superposition of the images taken by the two cameras in a pair.

corresponds to the location of the interaction in that direction. On the other hand, by inverting eq. 1, one can estimate the distance from the charge collection region (Y coordinate), and therefore localize the position of the primary interaction.

This technique allows a large sensitive area (64.90 mm × 70.18 mm per sensor) to be imaged by a relatively small number of channels (384 per detector half) with a spatial resolution that can be as low as a few tens of µm. Indeed, the position along the X coordinate can be estimated with a precision $\Delta X < 25$ µm. On the other hand, due to the presence of a discrete number of anodes, it is harder to evaluate Y, and therefore $\Delta Y < 6$ mm. Due to this very elongated error box, this technique is referred to as *1.5-D imaging* [73]. An unavoidable drawback of the charge cloud reconstruction is that the signal is split among multiple readout channels and therefore the electronic noise is added multiple times to total reconstructed charge, implying a noisy estimation of the photon energy.

It is worth noting that the properties of 1.5-D imaging require a special design of the coded mask, which therefore features rectangular pixels to match the spatial resolution of the sensors. As a consequence, the image generated by a WFM camera has an elongated PSF, with an angular resolution of $\Delta\theta_X < 5'$ and $\Delta\theta_Y < 5°$. To mitigate this, the WFM in its various configurations always presents pairs of aligned cameras rotated by 90° with respect to one another, so that each patch of the sky is imaged twice at the same time, and the two images may be superimposed to ensure the finer resolution along both directions (Fig. 11).

6. The Lunar Electromagnetic Monitor in X-rays

As anticipated at the end of Sec. 1.1, in recent years there has been a rise in interest in the exploration of the Moon, and in its use for scientific activities. In the specific context of high energy astrophysics and the study of transients, with a particular look at the identification of electromagnetic counterparts of gravitational wave events, the lunar surface presents some peculiarities that make it suitable for an X-ray observatory.

- The absence of an atmosphere allows X-ray and γ-rays to reach the ground, enabling the use of a ground-based facility instead of a free-flyer, with the consequent relaxation of mass and volume (and possibility power) constraints.

- By exploiting the Moon's rotation, the full sky becomes accessible to an observatory placed at the lunar equator (half of the sky at the poles). Moreover, the stable environment and nearly

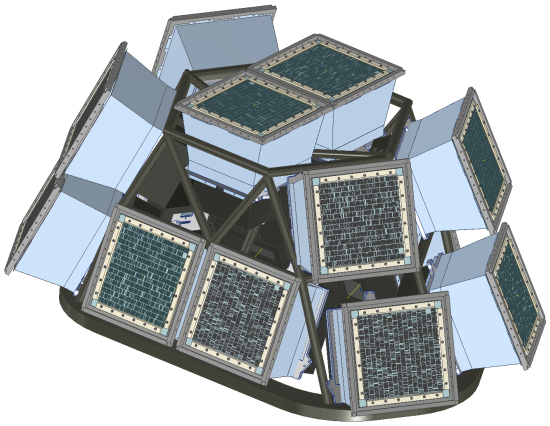

Figure 12: Current proposed camera configuration of LEM-X [74].

continuous operation (source occultations by the Earth are much rarer than for satellites on low-Earth orbits) make long observations possible, with the consequent improvement in location accuracy and reachable sensitivity. The relatively unobstructed lunar horizon also enables a large instantaneous FOV, up to 2π.

- The harsh but manageable radiation environment, dominated by solar particles and cosmic rays but far from those trapped in Earth's magnetosphere, limits the aging of sensors and readout electronics, implying a longer mission lifetime with good spectroscopic performances.

- The planned permanent human presence on the lunar surface opens up the possibility of continuous instrument serviceability, especially in combination with a modular design. A stable lunar facility may also further ease the requirements on volume, mass, and power.

In this context, the *Lunar Electromagnetic Monitor in X-rays* (LEM-X) is a proposed ground-based observatory on the surface of the Moon for the identification of X-ray transients, the localization of the electromagnetic counterparts of gravitational wave events, and the long-term monitoring of high-energy sources [75]. Active in the $2-50$ keV band, LEM-X will be made out of 7 pairs of WFM cameras (Sec. 5) in a dome-shaped structure to access the whole sky above the horizon at any given time (Fig. 12). The exact camera configuration and the location of the observatory on the Moon surface are currently under investigation, as they are subjected to a trade-off between the accessibility of the landing/construction site, the observability of the astrophysical sources and the feasibility of the structure itself from an engineering point of view [76].

At the present stage, the LEM-X project has been funded for the realization of a full detector plane of a single camera, consisting of four independent Detector Assemblies [74]. The design and optimization of all the other camera subsystems, as well as of the instrument as a whole, are also being carried out in parallel.

7. Conclusions

The next era of scientific discoveries in high-energy astrophysics will be dominated by simultaneous spectral and timing studies of transient phenomena, with valuable data being gathered on all timescales. Integration between observatories in the context of multi-messenger astronomy will also be key to unravel the mysteries of the most energetic phenomena in the universe. In addition, the return of humanity to the Moon and the possibility of a quasi-permanent presence will open up new and exciting scenarios for scientific advancements in all fields.

Traditional technologies have shown their limitations within this context. In this paper, we have reviewed some innovative instruments built around Silicon Drift Detectors coupled with innovative optical systems, that largely solve those shortcomings. The PixDD system can carry out high-resolution high-throughput spectral-timing observations with only mild cooling, and will be upgraded to cover the large focal planes typical of optics such as lobster-eyes (Sec. 2). The proposed configurations of the LAD feature an unprecedented effective area and low pile-up probability, to follow the spectral evolution of bright bursting sources (Sec. 3). The HERMES constellation will provide a distributed system for the detection and localization of Gamma-Ray Bursts via triangulation (Sec. 4). The WFM is a 2 sr-FOV compact camera for the detection and localization of transients with arcminute resolution (Sec. 5). The LEM-X observatory will be the first continuous all-sky monitor in X-rays operating from the surface of the Moon for the identification of electromagnetic counterparts of gravitational wave events (Sec. 6).

References

[1] B.P. Abbott et al., *Observation of Gravitational Waves from a Binary Black Hole Merger*, *Phys. Rev. Letters* **116** (2016) 061102 [1602.03837].

[2] B.P. Abbott et al., *Multi-messenger Observations of a Binary Neutron Star Merger*, *Astroph. Jour. Letters* **848** (2017) L12 [1710.05833].

[3] A. Goldstein et al., *An Ordinary Short Gamma-Ray Burst with Extraordinary Implications: Fermi-GBM Detection of GRB 170817A*, *Astroph. Jour. Letters* **848** (2017) L14 [1710.05446].

[4] E. Troja et al., *The X-ray counterpart to the gravitational-wave event GW170817*, *Nature* **551** (2017) 71 [1710.05433].

[5] IceCube Collaboration, *Evidence for High-Energy Extraterrestrial Neutrinos at the IceCube Detector*, *Science* **342** (2013) 1242856 [1311.5238].

[6] P. Mészáros, D.B. Fox, C. Hanna and K. Murase, *Multi-messenger astrophysics*, *Nature Reviews Physics* **1** (2019) 585 [1906.10212].

[7] A.L. Watts, W. Yu, J. Poutanen, S. Zhang, S. Bhattacharyya, S. Bogdanov et al., *Dense matter with eXTP*, *Science China Physics, Mechanics, and Astronomy* **62** (2019) 29503 [1812.04021].

[8] A. De Rosa, P. Uttley, L. Gou, Y. Liu, C. Bambi, D. Barret et al., *Accretion in strong field gravity with eXTP*, *Science China Physics, Mechanics, and Astronomy* **62** (2019) 29504 [1812.04022].

[9] J.J.M. in't Zand, E. Bozzo, J. Qu, X.-D. Li, L. Amati, Y. Chen et al., *Observatory science with eXTP*, *Science China Physics, Mechanics, and Astronomy* **62** (2019) 29506 [1812.04023].

[10] "Artemis accords." https://www.nasa.gov/artemis-accords.

[11] "ESA's moon exploration resources." https://lunarexploration.esa.int/explore.

[12] "JAXA's moon exploration resources." https://www.exploration.jaxa.jp/e/index.html.

[13] "CNSA's moon exploration resources." https://www.cnsa.gov.cn/english/n6465652/n6465653/c6810557/content.html.

[14] "ISRO's space program." https://www.isro.gov.in/spacesciexp.html.

[15] H. Wolter, *Spiegelsysteme streifenden Einfalls als abbildende Optiken für Röntgenstrahlen*, *Annalen der Physik* **445** (1952) 94.

[16] F. Jansen, D. Lumb, B. Altieri, J. Clavel, M. Ehle, C. Erd et al., *XMM-Newton observatory. I. The spacecraft and operations*, *Astronomy and Astrophysics* **365** (2001) L1.

[17] D.E. Zissa, *AXAF-1 high-resolution mirror assembly image model and comparison with x-ray ground-test image*, in *X-Ray Optics, Instruments, and Missions II*, R.B. Hoover and A.B. Walker, eds., vol. 3766 of *Society of Photo-Optical Instrumentation Engineers (SPIE) Conference Series*, pp. 36–50, Sept., 1999, DOI.

[18] F.A. Harrison, W.W. Craig, F.E. Christensen, C.J. Hailey, W.W. Zhang, S.E. Boggs et al., *The Nuclear Spectroscopic Telescope Array (NuSTAR) High-energy X-Ray Mission*, *Astrophysical Journal* **770** (2013) 103 [1301.7307].

[19] S.D. Bongiorno, J.J. Kolodziejczak, K. Kilaru, R. Eng, M. Stahl, W.H. Baumgartner et al., *Assembly of the IXPE mirror modules*, in *Optics for EUV, X-Ray, and Gamma-Ray Astronomy X*, S.L. O'Dell, J.A. Gaskin and G. Pareschi, eds., vol. 11822 of *Society of Photo-Optical Instrumentation Engineers (SPIE) Conference Series*, p. 118220Y, Sept., 2021, DOI.

[20] L. Strüder, U. Briel, K. Dennerl, R. Hartmann, E. Kendziorra, N. Meidinger et al., *The European Photon Imaging Camera on XMM-Newton: The pn-CCD camera*, *Astronomy and Astrophysics* **365** (2001) L18.

[21] M.J.L. Turner, A. Abbey, M. Arnaud, M. Balasini, M. Barbera, E. Belsole et al., *The European Photon Imaging Camera on XMM-Newton: The MOS cameras*, *Astronomy and Astrophysics* **365** (2001) L27 [astro-ph/0011498].

[22] N. Meidinger, R. Andritschke, W. Bornemann, D. Coutinho, V. Emberger, O. Hälker et al., *Report on the eROSITA camera system*, in *Space Telescopes and Instrumentation 2014: Ultraviolet to Gamma Ray*, T. Takahashi, J.-W.A. den Herder and M. Bautz, eds., vol. 9144 of *Society of Photo-Optical Instrumentation Engineers (SPIE) Conference Series*, p. 91441W, July, 2014, DOI.

[23] J. Kemmer and G. Lutz, *New detector concepts*, *Nuclear Instruments and Methods in Physics Research A* **253** (1987) 365.

[24] J. Kemmer, G. Lutz, U. Prechtel, K. Schuster, M. Sterzik, L. Strüder et al., *Experimental confirmation of a new semiconductor detector principle*, *Nuclear Instruments and Methods in Physics Research A* **288** (1990) 92.

[25] G. Lutz, R.H. Richter and L. Strüder, *Novel pixel detectors for X-ray astronomy and other applications*, *Nuclear Instruments and Methods in Physics Research A* **461** (2001) 393.

[26] N. Meidinger, M. Barbera, V. Emberger, M. Fürmetz, M. Manhart, J. Müller-Seidlitz et al., *The Wide Field Imager instrument for Athena*, in *Society of Photo-Optical Instrumentation Engineers (SPIE) Conference Series*, vol. 10397 of *Society of Photo-Optical Instrumentation Engineers (SPIE) Conference Series*, p. 103970V, Aug., 2017, DOI.

[27] M. Porro, L. Andricek, S. Aschauer, M. Bayer, J. Becker, L. Bombelli et al., *Development of the DEPFET Sensor With Signal Compression: A Large Format X-Ray Imager With Mega-Frame Readout Capability for the European XFEL*, *IEEE Transactions on Nuclear Science* **59** (2012) 3339.

[28] E. Gatti and P. Rehak, *Semiconductor drift chamber — An application of a novel charge transport scheme*, *Nuclear Instruments and Methods in Physics Research* **225** (1984) 608.

[29] T. Okajima, Y. Soong, E.R. Balsamo, T. Enoto, L. Olsen, R. Koenecke et al., *Performance of NICER flight x-ray concentrator*, in *Space Telescopes and Instrumentation 2016: Ultraviolet to Gamma Ray*, J.-W.A. den Herder, T. Takahashi and M. Bautz, eds., vol. 9905 of *Society of Photo-Optical Instrumentation Engineers (SPIE) Conference Series*, p. 99054X, July, 2016, DOI.

[30] K. Mercier, F. Gonzalez, D. Götz, M. Boutelier, N. Boufracha, V. Burwitz et al., *MXT instrument on-board the French-Chinese SVOM mission*, in *Space Telescopes and Instrumentation 2018: Ultraviolet to Gamma Ray*, J.-W.A. den Herder, S. Nikzad and K. Nakazawa, eds., vol. 10699 of *Society of Photo-Optical Instrumentation Engineers (SPIE) Conference Series*, p. 1069921, July, 2018, DOI.

[31] J. Bufon, M. Altissimo, G. Aquilanti, P. Bellutti, G. Bertuccio, F. Billè et al., *Large solid angle and high detection efficiency multi-element silicon drift detectors (SDD) for synchrotron based x-ray spectroscopy*, in *Synchrotron Radiation Instrumentation - SRI2018*, vol. 2054 of *American Institute of Physics Conference Series*, p. 060061, AIP, Jan., 2019, DOI.

[32] G. Bertuccio, M. Ahangarianabhari, C. Graziani, D. Macera, Y. Shi, M. Gandola et al., *X-Ray Silicon Drift Detector-CMOS Front-End System with High Energy Resolution at Room Temperature*, *IEEE Transactions on Nuclear Science* **63** (2016) 400 [2201.01698].

[33] M. Gandola, M. Grassi, F. Mele, I. Dedolli, P. Malcovati and G. Bertuccio, *The sparse readout RIGEL Application Specific Integrated Circuit for Pixel Silicon Drift Detectors in soft X-ray imaging space applications*, *Nuclear Instruments and Methods in Physics Research A* **1040** (2022) 167249 [2204.12778].

[34] F. Ceraudo, I. Dedolli, D. Cirrincione, E. Del Monte, F. Mele, F. Ambrosino et al., *Radiation-induced effects on the RIGEL ASIC*, *Nuclear Instruments and Methods in Physics Research A* **1037** (2022) 166903.

[35] M. Caselle, T. Blank, F. Colombo, A. Dierlamm, U. Husemann, S. Kudella et al., *Low-cost bump-bonding processes for high energy physics pixel detectors*, *Journal of Instrumentation* **11** (2016) C01050.

[36] Y. Evangelista, F. Ambrosino, M. Feroci, P. Bellutti, G. Bertuccio, G. Borghi et al., *Characterization of a novel pixelated Silicon Drift Detector (PixDD) for high-throughput X-ray astrophysics*, *Journal of Instrumentation* **13** (2018) P09011 [1808.08041].

[37] M. Sammartini, M. Gandola, F. Mele, G. Bertuccio, F. Ambrosino, P. Bellutti et al., *Pixel Drift Detector (PixDD) - SIRIO: an X-ray spectroscopic system with high energy resolution at room temperature*, *Nuclear Instruments and Methods in Physics Research A* **953** (2020) 163114.

[38] F. Ceraudo, F. Ambrosino, P. Bellutti, G. Bertuccio, G. Borghi, R. Campana et al., *PixDD: a multi-pixel silicon drift detector for high-throughput spectral-timing studies*, in *X-Ray, Optical, and Infrared Detectors for Astronomy X*, A.D. Holland and J. Beletic, eds., vol. 12191 of *Society of Photo-Optical Instrumentation Engineers (SPIE) Conference Series*, p. 1219116, Aug., 2022, DOI.

[39] I. Dedolli, F. Mele, F. Ceraudo, M. Gandola, M. Grassi, P. Bellutti et al., *Experimental Characterization of the RIGEL Sparse Readout ASIC for Soft X-Ray PixDD Detector*, in *2022 IEEE Nuclear Science Symposium and Medical Imaging Conference (NSS/MIC)*, pp. 1–3, 2022, DOI.

[40] C. Kenney, S. Parker, J. Segal and C. Storment, *Silicon detectors with 3-D electrode arrays: fabrication and initial test results*, *IEEE Transactions on Nuclear Science* **46** (1999) 1224.

[41] C.J. Kenney, J.D. Segal, E. Westbrook, S. Parker, J. Hasi, C. Da Via et al., *Active-edge planar radiation sensors*, *Nuclear Instruments and Methods in Physics Research A* **565** (2006) 272.

[42] A. Manazza, L. Gaioni, M. Manghisoni, V. Re, G. Traversi, S. Bettarini et al., *CMOS MAPS in a Homogeneous 3D Process for Charged Particle Tracking*, *IEEE Transactions on Nuclear Science* **61** (2014) 700.

[43] S. Zane and LOFT Detector's Group, *LOFT — Large Observatory for X-ray Timing*, *Journal of Instrumentation* **9** (2014) C12003 [1410.8681].

[44] A. Vacchi and LOFT Collaboration, *The LOFT mission concept*, *Nuclear and Particle Physics Proceedings* **297-299** (2018) 194.

[45] S. Zhang, A. Santangelo, M. Feroci, Y. Xu, F. Lu, Y. Chen et al., *The enhanced X-ray Timing and Polarimetry mission—eXTP*, *Science China Physics, Mechanics, and Astronomy* **62** (2019) 29502 [1812.04020].

[46] M. Feroci, G. Ambrosi, M. Antonelli, A. Argan, V. Babinec, M. Barbera et al., *The Large Area Detector for the eXTP mission*, in *Space Telescopes and Instrumentation 2024: Ultraviolet to Gamma Ray*, J.-W.A. den Herder, S. Nikzad and K. Nakazawa, eds., vol. 13093, p. 130931X, International Society for Optics and Photonics, SPIE, 2024, DOI.

[47] P.S. Ray et al., *STROBE-X: a probe-class mission for x-ray spectroscopy and timing on timescales from microseconds to years*, in *Space Telescopes and Instrumentation 2018: Ultraviolet to Gamma Ray*, J.-W.A. den Herder, S. Nikzad and K. Nakazawa, eds., vol. 10699 of *Society of Photo-Optical Instrumentation Engineers (SPIE) Conference Series*, p. 1069919, July, 2018, DOI [1807.01179].

[48] A.L. Hutcheson, M. Feroci, A. Argan, M. Antonelli, M. Barbera, J. Bayer et al., *Spectroscopic Time-Resolving Observatory for Broadband Energy X-ray high-energy modular array*, *Journal of Astronomical Telescopes, Instruments, and Systems* **10** (2024) 042503.

[49] "STROBE-X website." https://strobe-x.org.

[50] G. Lombardi, V. Mendes, A. Trois, G. Morgante, F. Ceraudo and R. Piazzolla, *The thermo-mechanical design of the module of the LAD instrument onboard the eXTP mission*, in *Space Telescopes and Instrumentation 2022: Ultraviolet to Gamma Ray*, J.-W.A. den Herder, S. Nikzad and K. Nakazawa, eds., vol. 12181, p. 121816Q, International Society for Optics and Photonics, SPIE, 2022, DOI.

[51] F. Ceraudo, J. Ge, Y. Evangelista, F. Muleri, M. Hanqi, X. Zhao et al., *Characterization of the NNVT capillary plate collimators*, *Journal of Instrumentation* **13** (2018) P09020.

[52] Z. Zhao, T. Luo, F. Ceraudo, M. Feroci, L. Li, J. Wang et al., *Characterization of the eXTP-LAD collimators*, *Experimental Astronomy* **57** (2024) 29.

[53] A. Nuti, F. Ceraudo, G. Della Casa, E. Del Monte, G. Dilillo, Y. Evangelista et al., *Development of a facility for high accuracy and precision characterization of Micro-Pore Optics collimators*, in *Space Telescopes and Instrumentation 2024: Ultraviolet to Gamma Ray*, J.-W.A. den Herder, S. Nikzad and K. Nakazawa, eds., vol. 13093 of *Society of Photo-Optical Instrumentation Engineers (SPIE) Conference Series*, p. 130936V, Aug., 2024, DOI.

[54] L. Li, T. Luo, Y. Xu, J. Wang, X. Cong, H. He et al., *Investigation of the optical performance of microchannel plate (MCP) collimators for the eXTP-LAD telescope*, *Nuclear Instruments and Methods in Physics Research A* **1070** (2025) 170059.

[55] A. Rachevski, G. Zampa, N. Zampa, R. Campana, Y. Evangelista, G. Giacomini et al., *Large-area linear Silicon Drift Detector design for X-ray experiments*, *Journal of Instrumentation* **9** (2014) P07014.

[56] F. Ceraudo, G.D. Casa, G. Bertuccio, W. Bonvicini, R. Campana, D. Cirrincione et al., *Improving the eXTP/LAD detector energy resolution with a novel sensor design*, in *Space Telescopes and Instrumentation 2024: Ultraviolet to Gamma Ray*, J.-W.A. den Herder, S. Nikzad and K. Nakazawa, eds., vol. 13093, p. 130936R, International Society for Optics and Photonics, SPIE, 2024, DOI.

[57] E. Del Monte, Y. Evangelista, E. Bozzo, F. Cadoux, A. Rachevski, G. Zampa et al., *The effect of the displacement damage on the Charge Collection Efficiency in Silicon Drift Detectors for the LOFT satellite*, *Journal of Instrumentation* **10** (2015) P05002 [1503.07682].

[58] G. Della Casa, F. Ceraudo, W. Bonvicini, R. Campana, D. Cirrincione, E. Del Monte et al., *Exploring the impact of total ionizing dose on the LAD detectors leakage current*, in *Space Telescopes and Instrumentation 2024: Ultraviolet to Gamma Ray*, J.-W.A. den Herder, S. Nikzad and K. Nakazawa, eds., vol. 13093 of *Society of Photo-Optical Instrumentation Engineers (SPIE) Conference Series*, p. 130936S, Aug., 2024, DOI.

[59] G. Zampa, E. Del Monte, E. Perinati, I. Rashevskaya, A. Rachevski, N. Zampa et al., *The effects of hyper-velocity dust-particle impacts on the LOFT Silicon Drift Detectors*, *Journal of Instrumentation* **9** (2014) P07015.

[60] F. Fiore, L. Burderi, M. Lavagna, R. Bertacin, Y. Evangelista, R. Campana et al., *The HERMES-technologic and scientific pathfinder*, in *Space Telescopes and Instrumentation 2020: Ultraviolet to Gamma Ray*, J.-W.A. den Herder, S. Nikzad and K. Nakazawa, eds., vol. 11444 of *Society of Photo-Optical Instrumentation Engineers (SPIE) Conference Series*, p. 114441R, Dec., 2020, DOI [2101.03078].

[61] Y. Evangelista, F. Fiore, R. Campana, G. Baroni, F. Ceraudo, G. Della Casa et al., *The HERMES (High Energy Rapid Modular Ensemble of Satellites) Pathfinder mission*, in *Space Telescopes and Instrumentation 2024: Ultraviolet to Gamma Ray*, J.-W.A. den Herder, S. Nikzad and K. Nakazawa, eds., vol. 13093 of *Society of Photo-Optical Instrumentation Engineers (SPIE) Conference Series*, p. 130931Z, Aug., 2024, DOI [2409.00989].

[62] M. Trenti, *The SpIRIT CubeSat: high energy astrophysics in harsh radiation environments and new technology demonstration*, in *43rd COSPAR Scientific Assembly. Held 28 January - 4 February*, vol. 43, p. 1507, Jan., 2021.

[63] A. Sanna, L. Burderi, T. Di Salvo, F. Fiore, A. Riggio, A. Gambino et al., *Timing techniques applied to distributed modular high-energy astronomy: the H.E.R.M.E.S. project*, in *Space*

Telescopes and Instrumentation 2020: Ultraviolet to Gamma Ray, J.-W.A. den Herder, S. Nikzad and K. Nakazawa, eds., vol. 11444 of *Society of Photo-Optical Instrumentation Engineers (SPIE) Conference Series*, p. 114444X, Dec., 2020, DOI [2101.03082].

[64] F. Fuschino, R. Campana, C. Labanti, Y. Evangelista, F. Fiore, M. Gandola et al., *An innovative architecture for wide band transient monitor on board the HERMES nano-satellite constellation*, in *Space Telescopes and Instrumentation 2020: Ultraviolet to Gamma Ray*, J.-W.A. den Herder, S. Nikzad and K. Nakazawa, eds., vol. 11444 of *Society of Photo-Optical Instrumentation Engineers (SPIE) Conference Series*, p. 114441S, Dec., 2020, DOI [2101.03035].

[65] Y. Evangelista, F. Fiore, F. Fuschino, R. Campana, F. Ceraudo, E. Demenev et al., *The scientific payload on-board the HERMES-TP and HERMES-SP CubeSat missions*, in *Space Telescopes and Instrumentation 2020: Ultraviolet to Gamma Ray*, J.-W.A. den Herder, S. Nikzad and K. Nakazawa, eds., vol. 11444 of *Society of Photo-Optical Instrumentation Engineers (SPIE) Conference Series*, p. 114441T, Dec., 2020, DOI [2101.03032].

[66] R. Campana, Y. Evangelista, F. Fiore, A. Guzmán, G. Baroni, G. Della Casa et al., *Design and development of the HERMES Pathfinder payloads*, in *Space Telescopes and Instrumentation 2024: Ultraviolet to Gamma Ray*, J.-W.A. den Herder, S. Nikzad and K. Nakazawa, eds., vol. 13093 of *Society of Photo-Optical Instrumentation Engineers (SPIE) Conference Series*, p. 130936F, Aug., 2024, DOI.

[67] G. Dilillo, E.J. Marchesini, G. Della Casa, G. Baroni, R. Campana, E. Borciani et al., *The HERMES calibration pipeline: MESCAL*, *Astronomy and Computing* **46** (2024) 100797 [2402.02937].

[68] S. Brandt et al., *The design of the wide field monitor for the LOFT mission*, in *Space Telescopes and Instrumentation 2014: Ultraviolet to Gamma Ray*, T. Takahashi, J.-W.A. den Herder and M. Bautz, eds., vol. 9144 of *Society of Photo-Optical Instrumentation Engineers (SPIE) Conference Series*, p. 91442V, July, 2014, DOI [1408.6540].

[69] M. Hernanz, M. Feroci, Y. Evangelista, A. Meuris, S. Schanne, G. Zampa et al., *The Wide Field Monitor (WFM) of the China-Europe eXTP (enhanced X-ray Timing and Polarimetry) mission*, in *Space Telescopes and Instrumentation 2024: Ultraviolet to Gamma Ray*, J.-W.A. den Herder, S. Nikzad and K. Nakazawa, eds., vol. 13093, p. 130931Y, International Society for Optics and Photonics, SPIE, 2024, DOI.

[70] R.A. Remillard, M. Hernanz, J. in't Zand, P.S. Ray, W. Bonvicini, S. Brandt et al., *The STROBE-X wide field monitor instrument*, *Journal of Astronomical Telescopes, Instruments, and Systems* **10** (2024) 042505.

[71] F. Ceraudo, G. Della Casa, G. Bertuccio, W. Bonvicini, R. Campana, D. Cirrincione et al., *Imaging and spectroscopic performances of the silicon drift detector of the wide field monitor*, in *Space Telescopes and Instrumentation 2024: Ultraviolet to Gamma Ray*, J.-W.A. den Herder, S. Nikzad and K. Nakazawa, eds., vol. 13093 of *Society of Photo-Optical Instrumentation Engineers (SPIE) Conference Series*, p. 130936U, Aug., 2024, DOI.

[72] F. Ceraudo, Y. Evangelista, M. Hernanz, J. in't Zand, L. Kuiper and A. Patruno, *Development of the end-to-end simulator of the WFM camera*, in *Space Telescopes and Instrumentation 2024: Ultraviolet to Gamma Ray*, J.-W.A. den Herder, S. Nikzad and K. Nakazawa, eds., vol. 13093 of *Society of Photo-Optical Instrumentation Engineers (SPIE) Conference Series*, p. 130936T, Aug., 2024, DOI.

[73] Y. Evangelista, R. Campana, E. Del Monte, I. Donnarumma, M. Feroci, F. Muleri et al., *Simulations of the x-ray imaging capabilities of the silicon drift detectors (SDD) for the LOFT wide-field monitor*, in *Space Telescopes and Instrumentation 2012: Ultraviolet to Gamma Ray*, T. Takahashi, S.S. Murray and J.-W.A. den Herder, eds., vol. 8443 of *Society of Photo-Optical Instrumentation Engineers (SPIE) Conference Series*, p. 84435P, Sept., 2012, DOI [1209.1501].

[74] F. Ceraudo, A. Nuti, G. Bertuccio, R. Campana, D. Cirrincione, G.D. Casa et al., *The detector assembly of the cameras of the Lunar Electromagnetic Monitor in X-rays (LEM-X)*, in *Space Telescopes and Instrumentation 2024: Ultraviolet to Gamma Ray*, J.-W.A. den Herder, S. Nikzad and K. Nakazawa, eds., vol. 13093, p. 130937N, International Society for Optics and Photonics, SPIE, 2024, DOI.

[75] E.D. Monte, F. Ceraudo, G.D. Casa, G. Dilillo, Y. Evangelista, M. Feroci et al., *Status of the Lunar Electromagnetic Monitor in X-rays (LEM-X)*, in *Space Telescopes and Instrumentation 2024: Ultraviolet to Gamma Ray*, J.-W.A. den Herder, S. Nikzad and K. Nakazawa, eds., vol. 13093, p. 130931U, International Society for Optics and Photonics, SPIE, 2024, DOI.

[76] A. Nuti, G. Dilillo, F. Ceraudo, G.D. Casa, E.D. Monte, Y. Evangelista et al., *The Lunar Electromagnetic Monitor in X-rays (LEM-X): optimization of the instrument layout and trade-off study for the observatory location on the Moon surface*, in *Space Telescopes and Instrumentation 2024: Ultraviolet to Gamma Ray*, J.-W.A. den Herder, S. Nikzad and K. Nakazawa, eds., vol. 13093, p. 130937O, International Society for Optics and Photonics, SPIE, 2024, DOI.

DISCUSSION

DENYS MALYSHEV: What is the advange of putting instruments on the Moon instead of the International Space Station?

FRANCESCO CERAUDO: An instrument on the Moon can in principle access the whole sky above the horizon at any given time and, depending on the location on the surface, it can observe the entire sky by taking advantage of the rotation of the Moon. In contrast, an instrument on the International Space Station (ISS) will experience Earth's occultations at every orbit and the Earth itself will be potentially in its field of view at any given time. Moreover, the ISS has to perform mandatory operations and maneuvers regardless of the scientific instruments operating onboard,

which will likely interrupt observations. For example, NICER only performs short acquisitions ($1-2$ ks) before it has to be repointed. This is simply not acceptable to an instrument whose purpose is to be an all-sky monitor to catch transients, that may very well occur in the inaccessible patches of sky or during non-operational times, if it was placed on the ISS.

ŞÖLEN BALMAN: How will the radiation damage be mitigated on the Moon and how? Or rather, what technology may be required to keep the detectors functioning nominally? Do we have this technology at the moment, or will we have it?

FRANCESCO CERAUDO: Radiation on the surface of the Moon will be primarily due to solar particles and cosmic rays, most of which will come through the same path as X-ray photons. For obvious reasons, shielding will not be very effective in this situation. Since from previous experimental studies it has emerged that detectors built with the same technology as LEM-X's mainly experience an increase in the leakage current due to displacement damage (e.g., no "hot channels"), and since leakage current also depends on the temperature of the sensors, the baseline mitigation strategy consists of regulating the operating temperature of the detectors. This will be done partly at the instrument level, for example by the choice of the site on the Moon surface, and partly at the detector level, by the use of active temperature control.

THOMAS SCHWEIZER: How will LEM-X reach the Moon? Where is it to be installed?

FRANCESCO CERAUDO: Means of transportations and the exact placement on the surface of the Moon are still under definition. Talks of a multi-project platform, as well as a dedicated mission are ongoing, both with the Italian Space Agency and with the industry. Regarding the location, this partially depends on whether LEM-X will be joining other instruments in a shared mission or be on its own. Moreover, every location has its advantages and drawbacks. For example, an equatorial site will experience more extreme temperature variations but allow all the sky to be accessed, whereas a polar site will lock away several sources but grant more stable environmental conditions.

DHEERAJ PASHAM: Isn't it more expensive to operate from the Moon compared to space?

FRANCESCO CERAUDO: LEM-X was originally proposed within the context of a quasi-permanent human presence on the Moon. With this in mind, part of the infrastructure will be shared between LEM-X and other facilities, thus lowering the burden of maintenance.

DHEERAJ PASHAM: Can PixDD go below 0.5 keV?

FRANCESCO CERAUDO: At the moment, the lower end of the energy band is mainly dictated by the readout electronics, as the 0.5 keV was set as a requirement for the ASIC. However, sensors built by our collaboration, with a different design but the same technology for the X-ray entrance window, have successfully detected the carbon K line at 277 eV. After tests on the low-energy

response are completed, as they are currently underway, an update on the ASIC requirement may be formulated.

SILVIA ZANE: Can you comment on why you said the MPO collimator is cheap? It may be a major cost in Europe (e.g. if built by Photonis).

FRANCESCO CERAUDO: MPO collimators are of course cheaper than older bulkier alternatives. Currently, a Chinese company, North Night Vision Technology Co. Ltd. (NNVT), is tasked with the design and production of MPOs, and they developed their technology adapting it from that of Micro-Channel Plates (MCP) used as light intensifiers for night vision devices. This means that a large portion of the production process already features a very high level of standardization, which drives down costs. Incidentally, this is the same company that produced the lobster-eye optics for the Einstein Probe space mission. Anyway, development of the LAD collimator is still underway to make the samples fully compliant with the instrument requirements.